Single Giant Vesicle Rupture Events Reveal Multiple Mechanisms of Glass-Supported Bilayer Formation

Chiho Hamai,* Paul S. Cremer,† and Siegfried M. Musser*
*Department of Molecular and Cellular Medicine, The Texas A&M University System Health Science Center, College Station, Texas; and †Department of Chemistry, Texas A&M University, College Station, Texas

ABSTRACT The formation of supported lipid bilayers (SLBs) on glass from giant unilamellar vesicles (GUVs) was studied using fluorescence microscopy. We show that GUV rupture occurs by at least four mechanisms, including 1), spontaneous rupture of isolated GUVs yielding almost heart-shaped bilayer patches (asymmetric rupture); 2), spontaneous rupture of isolated GUVs yielding circular bilayer patches (symmetric rupture); 3), induced rupture of an incoming vesicle when it contacts a planar bilayer edge; and 4), induced rupture of an adsorbed GUV when a nearby GUV spontaneously ruptures. In pathway 1, the dominant rupture pathway for isolated GUVs, GUVs deformed upon adsorption to the glass surface, and planar bilayer patch formation was initiated by rupture pore formation near the rim of the glass-bilayer interface. Expanding rupture pores led to planar bilayer formation in ~10–20 ms. Rupture probability per unit time depended on the average intrinsic curvature of the component lipids. The membrane leaflet adsorbed to the glass surface in planar bilayer patches originated from the outer leaflet of GUVs. Pathway 2 was rarely observed. We surmise that SLB formation is predominantly initiated by pathway 1 rupture events, and that rupture events occurring by pathways 3 and 4 dominate during later stages of SLB formation.

INTRODUCTION

Supported lipid bilayers (SLBs) have been widely studied as model systems for elucidating the intrinsic properties of lipids, membranes, and membrane proteins. Their importance stems from their amenability to a large number of surface analytical techniques, and their potential suitability for stabilizing membrane proteins in biosensor devices (1–5). In addition, one of our long-term goals is to construct supported and unsupported lipid bilayers from various cell membranes for structural, functional, and analytical studies. General problems with native membrane vesicles are that they do not rupture and fuse on a solid support, or when SLBs are made, the proteins are rendered immobile by adsorption to the surface. Our goal here was to investigate the lipid-dependent mechanisms responsible for vesicle rupture and bilayer fusion to form SLBs.

For pure phosphatidycholine (PC) bilayers, SLB formation is typically quite efficient and straightforward. PC phospholipid vesicles spontaneously adsorb to numerous solid surfaces, and vesicle rupture events and fusion of the adsorbed bilayer structures lead to a fairly homogeneous SLB, though small defects can occur (1,2,4,6–11). However, different lipid compositions and the presence of proteins can affect the efficiency of this SLB formation process (10,12,13). The current model is that the vesicles first adsorb and flatten due to favorable interactions with the surface, then possibly fuse together forming larger vesicles, and finally rupture to form SLBs (1,2,6–9). The basic mechanistic principles that control vesicle rupture, however, are poorly understood. The surface interaction energy, the intrinsic stability of the vesicle, and the multiple lipid structures simultaneously present at or near the surface during SLB formation (including incoming intact vesicles, adsorbed deformed vesicles, and edges of growing SLB patches) could all play crucial roles in determining the efficiency of vesicle rupture.

Bilayer structures allow assemblies of amphipathic lipid molecules to sequester hydrophobic tail domains away from the aqueous solution. Bilayer sheets either must expose the hydrophobic interior of the bilayer edge directly to the aqueous solvent, or the lipid molecules at the bilayer edge must arrange themselves into a sharply curved structure. Both of these arrangements are energetically unfavorable for most lipids. Thus, bilayer sheets in solution are unstable. Therefore, bilayers in solution typically form a typologically closed structure, such as a vesicle, which has no exposed edges. In contrast, for a planar SLB, no matter how large, there is always an edge. In most cases, a favorable surface adsorption energy can compensate for this edge energy (14). Since the edge energy of a circular adsorbed bilayer patch scales by the radius, R, and the adsorption energy scales by the area, or R^2, larger patches are more thermodynamically stable than smaller patches (14). Also, the fusion of two adsorbed vesicles is typically thermodynamically favorable (14), suggesting that vesicles may fuse before rupturing to yield a SLB patch. The final single SLB likely forms from many smaller SLBs that merge. The energetically unfavorable edges in these many small SLBs could play an important role in SLB growth, since it is more likely that growth occurs at the edges, rather than internally.

Submitted July 21, 2006, and accepted for publication November 30, 2006.

Address reprint requests to Siegfried M. Musser, Dept. of Molecular and Cellular Medicine, Texas A&M University Health Science Ctr., College Station, TX 77843. Tel.: 979-862-4128; Fax: 979-847-9481; E-mail: smusser@tamu.edu.

0006-3495/07/03/1988/12 $2.00

doi: 10.1529/biophysj.106.093831

SLB formation by vesicle fusion likely initiates from single-vesicle rupture events. Planar bilayer patches that form as a consequence of these rupture events likely expand by additional vesicle rupture events until the surface is covered by a single planar bilayer. What causes individual vesicles to rupture, and how lipids from additional vesicles merge with existing patches is poorly understood. Preparations of small unilamellar vesicles (SUVs) and large unilamellar vesicles (LUVs) with diameters of 50–200 nm are relatively homogeneous in size and lamellarity, and form relatively homogeneous SLBs (2,11,15,16). However, these vesicles are too small for visualizing global geometric changes by optical microscopy. In contrast, since shape changes of giant unilamellar vesicles (GUVs) with diameters of a few micrometers are easily visualized, we anticipated that direct visualization of GUV rupture events could provide insight into the mechanistic principles behind SLB formation. Of practical importance is the fact that membranes purified from biological systems typically have dimensions closer to GUV dimensions ($\geq \sim 1\ \mu$m) than to SUV or LUV dimensions (17–19). Thus, SLB formation from GUVs is more directly applicable to understanding the potential for SLB formation from biological membranes.

In this article, we describe GUV rupture mechanisms that occur during SLB formation on a glass surface. GUV rupture was monitored by fluorescence microscopy at a time resolution as fast as 2 ms. We show that isolated GUVs yield planar bilayer patches within ~10–20 ms of rupture pore formation. For isolated GUVs, rupture was a spontaneous event that appeared to depend on the formation of a sufficiently large pore within the adsorbed vesicle. The outer membrane leaflet of the GUV became the leaflet closest to the surface in the resultant bilayer patch, indicating that the bilayer of an adsorbed vesicle simply opens up and flattens. Vesicle rupture was also catalyzed by contact with the edge of a bilayer patch. GUV rupture was inhibited by high - negative-curvature lipids, suggesting that the activation barrier to rupture was determined largely by the edge energy of the rupture pore.

METHODS

Materials

1,2-dioleoyl-*sn*-glycero-3-phosphocholine (DOPC), 1,2-dioleoyl-*sn*-glycero-3-phosphoethanolamine-*N*,*N*-dimethyl (DOPE-Me_2), 1,2-dioleoyl-*sn*-glycero-3-phosphoethanolamine-*N*-methyl (DOPE-Me), 1,2-dioleoyl-*sn*-glycero-3-[phospho-*rac*-(1-glycerol)] (sodium salt) (DOPG), and 1-oleoyl-2-hydroxy-*sn*-glycero-3-phosphocholine (Lyso-PC) were purchased from Avanti Polar Lipids (Alabaster, AL). Texas Red (TR) 1,2-dihexadecanoyl-*sn*-glycero-3-phosphoethanolamine, triethylammonium salt (TR-DHPE), 5-(and-6-)-carboxyfluorescein (CF) mixed isomers, succinimidyl 6-(*N*-(7-nitrobenz-2-oxa-1,3-diazol-4-yl)amino)hexanoate (NBD succinimide), anti-dinitrophenyl antibody (anti-DNP, from rabbit), and the 25 amino acid transmembrane peptide $KR_2L_{19}R_2K$ were purchased from Invitrogen (Carlsbad, CA). The C- and N-termini of the peptide were blocked by acetyl and amide groups, respectively. Sodium dithionite (technical grade, 85%) and *N*-(NBD-aminocaproyl)-1,2-dipalmitoyl-*sn*-glycero-3-phosphoethanolamine sodium salt (NBD-cap PE) were purchased from Sigma (St. Louis, MO). All the chemicals were used as received, except for the peptide. Glass slides (22 × 22 mm, No. 1, or 24 × 60 mm, No. 1½) were purchased from VWR Scientific (West Chester, PA). High vacuum grease (Dow Corning, Midland, MI) was used to construct flow chambers.

Preparation of GUVs

GUVs were prepared as described previously (20), with minor modifications. Since charged lipids raise the yield of unilamellar vesicles (20), ~10 mol % of DOPG (a negatively charged lipid) was added to all GUV preparations. The yield of unilamellar vesicles decreased in the presence of salt and yet ions were necessary to adsorb GUVs to glass, presumably to shield the negatively charged vesicle surface from the negatively charged glass surface. Therefore, to prevent osmotic shock upon salt addition after GUV formation, 0.2 M sucrose (0.2 osmolar) was used to hydrate lipids for most GUV preparations. The resultant GUV solutions (0.8–1.6 mg/mL lipid) were diluted to 0.008–0.1 mg/mL lipid in 50 mM KCl, 10 mM HEPES, 1 mM Na_2EDTA, and 84 mM sucrose, pH 8.0 (Buffer A, ~0.21 osmolar) before adsorption to glass.

TR-DHPE, NBD-cap PE, and NBD_2-peptide were added to GUV preparations as fluorescent membrane markers. Phospholipid stock solutions were made with chloroform and stored at −80°C. Solutions of phospholipids and a fluorescent marker were mixed at the desired compositions, the solvent was removed under a stream of nitrogen, and the residue was dried under house vacuum for 1–2 h. The dried lipid films were hydrated as described above. The GUV clusters obtained after a 10-min hydration period were uniformly dispersed by gentle shaking.

Carboxyfluorescein (CF) was encapsulated in some GUVs as a lumenal marker. For these GUVs, lipids were hydrated in 10 mM CF, 5 mM HEPES, 185 mM sucrose, pH 8.0 (~0.22 osmolar), at a lipid concentration of 0.8 mg/mL. The preparations were incubated at 42°C for 1 h to fully hydrate the lipids. GUV clusters were then uniformly dispersed by gentle shaking. External CF molecules were removed by dialysis (60-kDa molecular mass cut-off) against 1400 volumes of 5 mM HEPES, 195 mM sucrose, pH 8.0 (Buffer B, ~0.21 osmolar) at 4°C. The dialysate was exchanged 1 h and 4 h after the dialysis was started, and the dialysis was continued overnight. According to the absorbance at 492 nm (GUVs + 1 mM Triton X-100), ~99% of the CF was removed by dialysis. The CF-containing GUVs were adsorbed to glass in Buffer B.

Phospholipid compositions in GUVs are expressed as mole ratios within the nonfluorescent lipids: e.g., DOPC/DOPG (9:1) labeled with 0.5 mol % TR-DHPE denotes a lipid composition of 89.55% DOPC, 9.95% DOPG, and 0.5% TR-DHPE.

Fluorescence microscopy

A Zeiss Axiovert 200M fluorescence microscope equipped with two CCD cameras (Cascade 512B and Cascade 128+, Photometrics, Tucson, AZ) was used to image GUVs and glass-adsorbed bilayer structures. Samples were illuminated with a 100-W mercury-arc lamp and imaged at magnifications of 100× or 160× by combining a 1.45-numerical aperture 100× oil-immersion objective with 1.0× or 1.6× optovars, respectively. The filter sets used for NBD and TR excitation were FF01-482/35:FF506-Di02-25×36:FF01-536/40 (Semrock, Rochester, NY) and HQ580/20:Q595LP:HQ630/60 (Chroma, Rockingham, VT), respectively. Pixel sizes for the Cascade 512B and Cascade 128+ cameras are 16 × 16 μm and 24 × 24 μm, respectively. With the Cascade 512B camera, data were collected at 9, 12, and 23 ms/frame using 100 × 100, 150 × 150, and 200 × 200 pixel areas, respectively. With the Cascade 128+ camera, full-frame data (128 × 128 pixels) were collected at 2 ms/frame.

Glass coverslips were cleaned before use as described earlier (10). GUVs were incubated with glass coverslip surfaces by depositing GUV solutions

(0.008–0.1 mg/mL lipid) into poly(dimethylsiloxane) chambers (attached to the coverslips through light pressure).

Estimation of the average intrinsic curvature

The average intrinsic curvature ($C_{0,ave}$) for lipid mixtures was estimated through weighted arithmetical averaging of the intrinsic curvatures of the component lipids:

$$C_{0,ave} = \sum_j X_j C_{0,j},$$

where X_j and $C_{0,j}$ are the mole fraction and the intrinsic curvature, respectively, for each component lipid (10). C_0 values were estimated as 0.26, −0.11, −0.23 and −0.35 nm^{-1} for Lyso-PC, DOPC, DOPE-Me_2, and DOPE-Me, respectively (10,21–23). The GUVs used for examining the effect of intrinsic curvature all contained 9.95 mol % DOPG and 0.5 mol % TR-DHPE. Since values for $C_{0,DOPG}$ and $C_{0,TR\text{-}DHPE}$ are not available, we approximated the average intrinsic curvature value by not including the contributions of DOPG and TR-DHPE, i.e., $C'_{0,ave} = C_{0,ave} - 0.0995C_{0,DOPG} - 0.005C_{0,TR\text{-}DHPE}$. The consequence of this approximation is that all the abscissa values in see Fig. 5 are offset by the same unknown amount.

Experimental values

Values are quoted as the mean ± standard error.

RESULTS

Identification of unilamellar and multilamellar GUVs and planar bilayer patches

GUV samples contained unilamellar and multilamellar vesicles. To preclude the interbilayer interactions that possibly occurred within a multilamellar vesicle, we determined the lamellarity of vesicles based on their appearance in microscopic images. DOPC/DOPG (9:1) GUVs (~2–8 μm diameter) labeled with 0.5 mol % TR-DHPE were deposited onto a glass coverslip (Fig. 1). At the resolution of light microscopy (~260 nm), the vesicles were spherical before adsorption; this was expected since the osmotic pressures inside and outside the vesicles were approximately equal (from ~0.2 to ~0.22 osmolar; see Methods). As noted earlier (24), a GUV typically adapts its volume such that the interior and exterior osmotic pressures are essentially equal. Epifluorescence images were used to identify adsorbed lipid structures. In general, three types of immobile features were observed. These features were characterized by obtaining images at varying focal planes above the glass surface (Fig. 1, *A–D*). Two features showed circular fluorescence distributions with sharper and brighter edges a few micrometers above the surface (Fig. 1, *B* and *C*). The fluorescence of these circular features became fuzzy and the diameter eventually decreased to zero when the focal plane was further raised above the surface (Fig. 1 *D*). These data are consistent with the hypothesis that the circular shapes arise from adsorbed vesicles, and we therefore assumed that these circular patterns were images of GUVs. The substructural

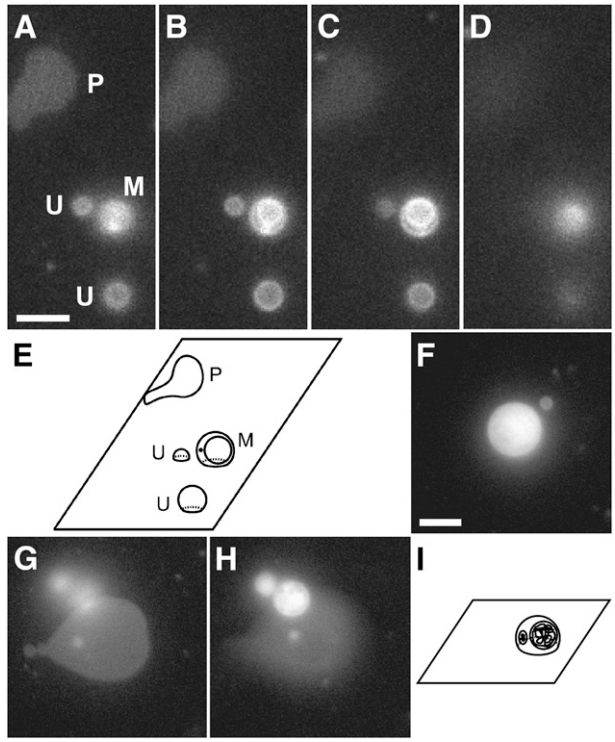

FIGURE 1 Distinguishing characteristics of planar bilayers, unilamellar vesicles, and multilamellar vesicles. DOPC/DOPG (9:1) GUVs labeled with 0.5 mol % TR-DHPE were adsorbed to a glass coverslip and visualized using Texas Red fluorescence emission. Unless otherwise noted, the focal plane was the glass surface. Scale bar in *A* and *F*, 5 μm. (*A–D*) A series of focal planes of the same coverslip-adsorbed GUV sample, with the focal plane 0, 1, 2, and 4 μm, respectively, above the glass surface. A planar bilayer, two unilamellar vesicles, and a multilamellar vesicle in *A* are marked P, U, and M, respectively. (*E*) Schematic illustration of the planar bilayer and the vesicles observed in *A–D*. (*F–H*) Rupture of a multilamellar GUV. (*F*) An adsorbed GUV. (*G*) The lipid structures in *F* after GUV rupture. A planar bilayer and the fuzzy outline of additional lipid structures above the surface are visible. (*H*) The lipid in *F* after GUV rupture at a focal plane above the surface. The internal lipid structures were identified as vesicles, indicating that the original GUV was multilamellar. The focal plane is 2.7 μm above the glass surface. (*I*) Schematic illustration of the adsorbed GUV in *F*. Cut-away views show the multilamellarity.

pattern of the circular shapes was used to judge lamellarity. The features that contained additional circular shapes inside the main circular pattern were designated multilamellar (*M*), whereas a single homogeneous circular fluorescence pattern was assumed to arise from a unilamellar (*U*) GUV (schematically illustrated in Fig. 1 *E*). In contrast to the circular shapes observed for the U and M features, other features were generally noncircular, and were sharpest and brightest in the glass-surface focal plane. These data suggested that these features did not contain lipid structures at substantial distances from the glass surface. We concluded that these features arose from planar bilayer patches (*P*) that resulted from GUVs that had ruptured on the surface.

The lamellarity of adsorbed vesicles was further confirmed by observation of the vesicle rupture process. When GUVs

ruptured forming a planar bilayer patch, mobile spherical spots similar to the U and M features were sometimes observed diffusing above the bilayer patch area (Fig. 1, *F–H*). These data are consistent with the hypothesis that when multilamellar GUVs rupture, internal vesicles are released from within the large vesicles that rupture. Thus, we assumed that the release of the interior contents of multilamellar vesicles could be directly visualized and that the observation of these contents as vesicles confirmed that the original GUV was multilamellar. If no internal structures were observed before rupture or no vesicular contents were observed upon rupture, the original GUV was deemed to be unilamellar.

Two rupture pathways for isolated GUVs at a high TR-DHPE concentration

For isolated DOPC/DOPG (9:1) GUVs, two distinct classes of bilayer patch shapes were observed upon vesicle rupture (Fig. 2): isolated bilayer patches were either asymmetric (almost heart-shaped) or symmetric (nearly circular). Since the initiation site for vesicle rupture was near the bilayer adsorbed region (asymmetric patches) or near the apex of the adsorbed structure (symmetric patches) rather than randomly distributed over the surface of the vesicle, we concluded that the two resultant patch shapes were diagnostic for distinct rupture mechanisms.

To directly visualize GUV rupture at 500 frames/s (fps), 3 mol % TR-DHPE was required to obtain a sufficiently intense fluorescence signal. In the major isolated GUV rupture pathway, a point on the circular rim of the fluorescence area defined by the adsorbed GUV became a point on the boundary of a planar bilayer patch that formed upon rupture, within the error of the measurements (Fig. 2 *A*). The common boundary point appeared to define, or be very near, the initiation point of the rupture process. A decrease in fluorescence per unit area was observed upon rupture, and this fluorescence decrease began near the common boundary point and expanded outward from this point to the entire area in ~10–20 ms. Since an epifluorescence image of an adsorbed vesicle can contain fluorescence intensity contributions from multiple bilayers (due to the large focal plane thickness relative to the height of the vesicle), whereas the fluorescence intensity pattern for a planar bilayer disk arises from a single bilayer, the fluorescence intensity per unit area was expected to decrease upon vesicle rupture. In addition, the area of the adsorbed bilayer structure is expected to increase during this rupture process. These predictions are supported by the observed images of the rupture process. Further, these data are consistent with a model in which vesicle rupture initiated near the rim of the adsorbed vesicle area, and continued expansion of a rupture pore led to an adsorbed planar bilayer patch (Fig. 2 *B*). This rupture process was deemed asymmetric for two reasons: 1), the center of mass of the adsorbed region for the intact vesicle and that of the resultant planar bilayer patch were significantly different

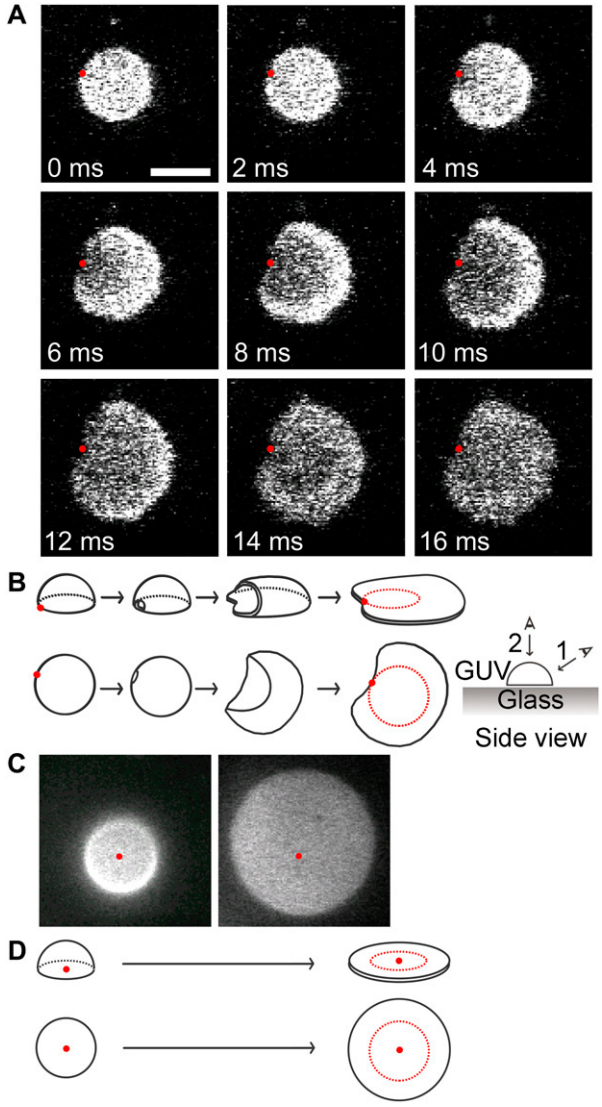

FIGURE 2 Rupture mechanisms for isolated GUVs. For all images, the focal plane was the glass surface. Scale bar in *A*, 5 μm; same scale for all images. (*A*) The major isolated rupture pathway. This image sequence, collected at 500 fps, shows that the changes in the geometry of the fluorescence pattern and in the average fluorescence intensity per unit area are consistent with the rupture of a single glass-adsorbed GUV. The red dots are in identical locations in each image and demonstrate that the observed fluorescence emission patterns have a common edge point. This edge point appears to be at or near the point at which rupture was initiated. A movie is available online in Supplementary Material (Fig2A.mov). (*B*) Schematic illustration of the rupture process shown in *A*. Two viewpoints are shown: (*upper*) viewpoint 1 is from the side of the vesicle, but looking down upon the surface; (*lower*) viewpoint 2 is from above the vesicle. Red dots have the same meaning as in *A*. The red circle on the final planar bilayer patch identifies the boundary of the surface-adsorbed lipid structure before rupture. (*C*) The minor isolated rupture pathway. A glass-adsorbed GUV (*left*) formed a planar bilayer patch (*right*) that was circular, with approximately the same center as the original adsorbed lipid structure. The location of the center of the circular fluorescence distribution in the left image is identified in both images by the red dot. Integration time, 64 ms. Time between images, ~8 min. (*D*) Schematic illustration of the rupture process shown in *C*. As in *B*, two viewpoints are shown. The red circles and red dots have the same meanings as in *B* and *C*, respectively.

(a geometrical consequence of the shared boundary point of the GUV adsorbed area and the larger bilayer patch area); and 2), the planar bilayer patches formed were almost heart-shaped, rather than circular.

In addition to the above rupture process, a second isolated GUV rupture pathway for DOPC/DOPG (9:1) GUVs containing 3 mol % TR-DHPE was observed. For this second pathway, the centers of the planar bilayer patches were near the centers of the original GUV adsorbed areas (Fig. 2, *C* and *D*). In addition, the planar bilayer patches formed were approximately circular. Thus, this rupture process was deemed symmetric. This rupture process is distinct from the asymmetric rupture process in that there is no common boundary point for the adsorbed areas before and after rupture. The symmetric rupture patterns are consistent with rupture initiation from near the apex of the adsorbed vesicle, followed by an approximately equal spreading around the entire initial absorbed area. Presumably due to the infrequency of rupture by this second mechanism, the rupture process itself was never directly observed at high time resolution, but rather inferred from lower time-resolution measurements. By collecting longer image sequences over a larger area, the conversion of isolated adsorbed vesicles to planar bilayer patches (larger fluorescence areas with reduced average fluorescence intensities) was more readily detected at 15.6 fps. Of 39 rupture events, 36 GUVs ruptured by the asymmetric pathway. The remaining three GUVs ruptured symmetrically. Thus, these data support the existence of two mechanistically distinct rupture pathways for isolated GUVs, which are distinguished visually by geometrical characteristics (shape as well as edge and center of mass location) of the planar bilayer patch area formed relative to the original adsorbed GUV area.

One rupture pathway for isolated GUVs at a low TR-DHPE concentration

Since high concentrations of TR-DHPE promote vesicle rupture on a glass surface (10), we next examined whether multiple isolated vesicle rupture pathways could be observed at 0.5 mol % TR-DHPE. At this low TR-DHPE concentration, the fluorescence signal was too weak to directly observe vesicle rupture at 500 fps. However, since the geometry of the bilayer patches that resulted from isolated GUV ruptures were diagnostic for the rupture pathway at 3 mol % TR-DHPE, these parameters were considered diagnostic for the rupture pathway at 0.5 mol % TR-DHPE. Thus, the rupture of GUVs with 0.5 mol % TR-DHPE was observed at 43–111 fps. For 66 rupture events, a common boundary point was shared by all planar bilayer patches and the corresponding original adsorbed vesicle area, as depicted in Fig. 2 *A*. Thus, we conclude that all, or nearly all, GUVs with 0.5 mol % TR-DHPE rupture by the asymmetric pathway. Further, we conclude that high concentrations of TR-DHPE increased the probability of symmetric rupture. Inversely, nonfluorescent DOPC/DOPG (9:1) GUVs are predicted to rupture almost exclusively by the asymmetric pathway. The symmetric rupture events observed with 3% TR-DHPE most likely resulted from a general bilayer instability at high TR-DHPE concentrations, consistent with earlier results (6). In contrast, the asymmetric rupture events likely occurred due to the high bilayer curvature at the surface interface.

Release of GUV contents upon rupture

To further confirm that the changes in fluorescence patterns observed for isolated GUVs were indeed vesicle rupture events and to investigate the mechanism of release of the GUVs' contents, we monitored the release of 10 mM CF that was encapsulated in DOPC/DOPG (9:1) GUVs labeled with 0.5 mol % TR-DHPE (Fig. 3). The TR-DHPE fluorescence signal was used to identify adsorbed GUVs. The CF fluorescence signal was then monitored during vesicle rupture at 500 fps. Since the GUV-encapsulated CF fluorescence intensity was highest in a focal plane above the glass, the CF fluorescence was first measured in successive focal planes above the surface separated by 0.2 μm. The focal plane that yielded the greatest CF fluorescence intensity was chosen to monitor vesicle rupture. Shortly after the CF fluorescence intensity rapidly dropped to baseline (in $<$ 200 ms), we examined the TR-DHPE fluorescence emission to check for the presence of a planar bilayer patch. Typical data are shown in Fig. 3, *A–C*. We observed 10 rupture events for GUVs containing CF. In all 10 cases, loss of CF appeared to coincide with vesicle rupture. In addition, all GUVs ruptured by the asymmetric pathway, as evidenced by the geometry of the planar bilayer patches formed. During the time interval in which the GUVs ruptured, the CF fluorescence distribution remained approximately circular, though it increased in size, and the center of the distribution invariably shifted away from the point at which rupture appeared to have initiated. After vesicle rupture, the CF fluorescence intensity decayed to background. These data are consistent with a picture in which the lumenal contents of the GUV shifted away from the rupture initiation site, perhaps dragged by the bilayer shell as it adsorbed to the glass surface. The decay of the CF fluorescence intensity due to CF diffusion after vesicle rupture was significantly slower than the vesicle rupture process, indicating that bilayer patch formation was driven faster than diffusion by a highly cooperative mechanism. To be more quantitative, note that the diffusion constant for TR-DHPE in our SLBs was $\sim$1–2 $\mu m^2/s$, predicting one-dimensional movement of $\sim$0.2 μm in $\sim$10 ms; in contrast, the adsorbed bilayer front in Fig. 2 *A* advanced up to $\sim$3.4 μm in 10 ms (to one-dimensionally diffuse this distance in 10 ms in the absence of a bias requires a diffusion constant of $>$ 500 $\mu m^2/s$, $\sim$100-fold higher than that for a lipid in an unsupported bilayer (25)). An adsorbed GUV's internal osmotic pressure could potentially be larger than that in solution due to the decrease in lumenal volume generated by vesicle adsorption and flattening. Since we did not observe

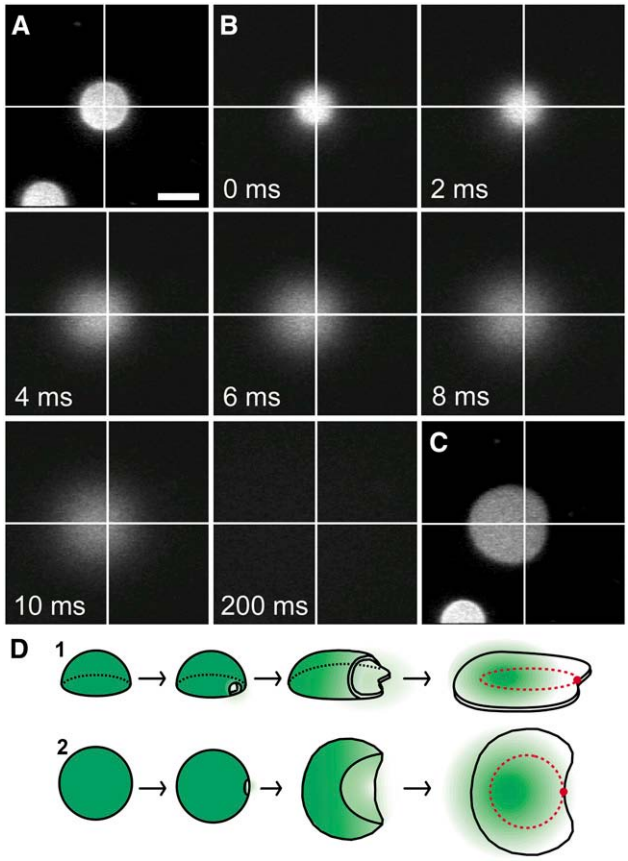

FIGURE 3 The release of GUV contents upon rupture. The rupture of GUVs was monitored by CF fluorescence intensity for DOPC/DOPG (9:1) GUVs containing 0.5 mol % TR-DHPE. Unless otherwise noted, the focal plane was the glass surface and the frame integration time was 64 ms. Scale bar in *A*, 5 μm; same scale for all images. (*A*) TR fluorescence intensity for an adsorbed GUV. (*B*) The CF (10 mM internal concentration) fluorescence intensity (observed at 500 fps) before, during, and after rupture of the GUV in *A*. The CF distribution begins to widen at 2 ms, indicating the release of CF molecules to the bulk solution. The focal plane is 2 μm above the glass surface. (*C*) TR fluorescence intensity for the planar bilayer patch observed 1–2 min after the data in *B* were obtained. For *A–C*, the crossing point of orthogonal white lines in each image marks the center of the circular fluorescence area in *A*. (*D*) Schematic illustration (two views) of the rupture process imaged in *A–C*. The rupture is modeled after Fig. 2 *B*. Green color shows the distribution of the CF dyes.

a plume of CF escaping from the rupture pore, we conclude that a significant internal osmotic pressure was not present in GUVs at the time of rupture. Leakage of solvent and/or solutes likely occurred before rupture, equalizing the internal and external pressures. These data are consistent with a rupture process that is initiated at a single rupture pore, and that proceeds by simultaneous expansion of the rupture pore and adsorption of the lipid bilayer to the glass surface (Fig. 3 *D*).

Area increase upon GUV rupture

To confirm that the sudden geometrical changes we observed were consistent with the rupture of a single GUV, we analyzed the total fluorescent area in the glass-surface focal plane before and after the geometrical changes. For 62 events, the glass-adsorbed bilayer area increased around two- to threefold upon vesicle rupture (Supplementary Material, Fig. S1). The glass-adsorbed bilayer area is expected to at least double when a single GUV ruptures (rupture of a fully flattened, ''pancaked'' vesicle). Thus, these data are consistent with the hypothesis that the geometrical changes described above that occurred in ~10–20 ms were a consequence of the rupture of a single GUV.

Fluorescence quenching of NBD-cap PE and an NBD-labeled transmembrane peptide by anti-DNP antibodies in planar bilayer patches

Three distinct possibilities exist for the distribution of lipids in a planar bilayer patch relative to the original adsorbed vesicle. First, the vesicle rupture process could be similar to a flower bud opening, such that the vesicle opens through the widening of a pore concurrent with adsorption of the outer leaflet to the surface, and the inner leaflet becomes exposed to the bulk solution. Second, the vesicle could somehow rupture such that the inner leaflet adsorbs to the surface leaving the outer leaflet exposed to the bulk solution. And third, the lipids in the two leaflets could become completely or partially scrambled before, during, or after rupture such that each of the two leaflets in the planar bilayer patch contain lipids from both the inner and outer leaflets of the original vesicle. Using antidinitrophenol (anti-DNP) antibodies to quench the NBD fluorescence of NBD-cap PE and an NBD-labeled transmembrane peptide, we conclude that the bulk of the membrane leaflet adsorbed to the glass surface in planar bilayer patches originated from the outer vesicle leaflet. In addition, NBD-cap PE lipids appeared able to migrate from the adsorbed membrane leaflet to the membrane leaflet exposed to the bulk solution by diffusing through a highly curved lipid structure at the bilayer edge (Supplementary Material).

Fluidity of planar bilayer patches

The fluidity of SLBs is normally examined by fluorescence recovery after photobleaching (FRAP) experiments (26,27). To obtain accurate lipid diffusion constants, normal FRAP analysis requires rapid photobleaching of a small area, which only accounts for a small fraction of the total area, and assumes an infinite reservoir of nonphotobleached fluorescent lipids. Due to the small size of planar bilayer patches, we could not meet these requirements. However, lipid fluidity could be confirmed as follows. When the rupture of a TR-DHPE-labeled GUV was recorded under relatively high illumination (40–140 μW at the specimen plane for these fluidity experiments; 1–3 μW for other experiments), a photobleached (dark) spot was clearly observed on the planar bilayer patch shortly after the rupture (Fig. 4 *A*). These data

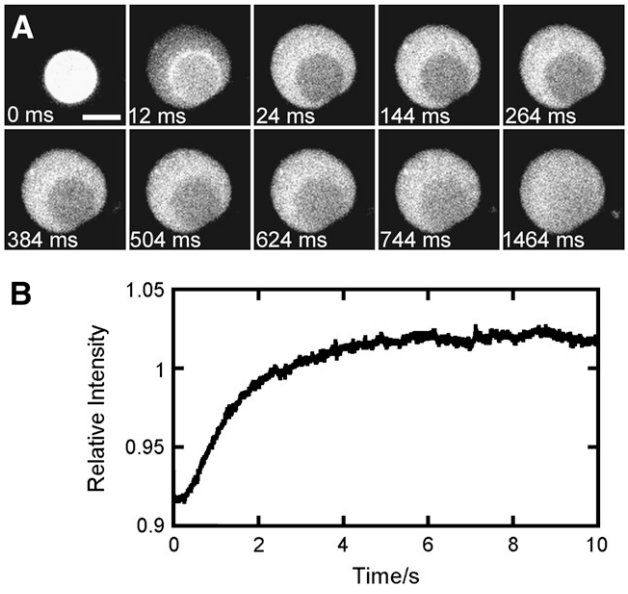

FIGURE 4 Fluidity of planar bilayer patches. FRAP data obtained for a DOPC/DOPG (9:1) GUV labeled with 0.5 mol % TR-DHPE. (*A*) The nonhomogeneous fluorescence intensity pattern observed immediately after GUV rupture at high illumination intensity. The surface-adsorbed GUV (the first frame in the image sequence is arbitrarily labeled 0 ms) asymmetrically ruptured during the 12-ms frame, yielding a fully formed planar bilayer patch by 24 ms. The later images show fluorescence recovery in the photobleached area that is observed in the 24-ms image. The photobleached area coincides with the bilayer-surface interaction area observed at 0 ms. During the 12-ms frame, the fluorescence intensities from the adsorbed GUV and the planar bilayer were both observed, since the 83.3 fps acquisition rate was not fast enough to resolve the rupture event. When six frames from Fig. 1 *A* (which shows a rupture event imaged at 500 fps) were combined to yield a single 12-ms frame, a similar intensity pattern to that observed in the 12-ms frame shown here was obtained, consistent with the interpretation that rupture occurred within the 12-ms frame. Focal plane, the glass surface; integration time, 12 ms; illumination intensity, 140 μW; scale bar, 5 μm. (*B*) Half-time for fluorescence recovery. The curve shows the time dependence ($t_{1/2} = 1.3$ s) of the relative fluorescence intensity (the average intensity for the photobleached area divided by the average intensity for the area surrounding the photobleached region) for the rupture event in *A*. The $t_{1/2}$ for 14 different rupture events for GUVs of different sizes ranged from 1.0 to 2.4 s. Time 0 s corresponds to 24 ms in *A*.

can be explained by the fact that the excitation illumination was focused at the glass surface, and thus, for an intact adsorbed GUV, the TR-DHPE lipids within the glass-adsorbed region were more likely than those elsewhere within the GUV to be photobleached. The fluorescence intensities arising from such dark spots recovered to a similar intensity as that arising from the remainder of the bilayer patch with a half-time ($t_{1/2}$) of ~1–2.4 s (Fig. 4 *B*). An accurate TR-DHPE diffusion constant cannot be obtained from these data by FRAP analysis since the reservoir of nonphotobleached fluorescent lipids is severely limited. For comparison, however, the TR-DHPE diffusion constants measured in SLBs formed from DOPC and DOPC/DOPG (9:1) LUVs as described previously (10) using a 23-μm-diameter photobleached area were 2.1 ± 0.1 μm^2/s (with mobile fraction, $F = 1$) and 1.2 ± 0.2 μm^2/s ($F = 0.8$), respectively. These data predict a $t_{1/2}$ of 1–2 s for a 6.2-μm-diameter spot (e.g., as in Fig. 4 *A*) surrounded by a bilayer with an infinite reservoir of TR-DHPE with a diffusion constant of 1–2 μm^2/s (27). This $t_{1/2}$ is similar to that observed for FRAP recovery in the bilayer patches (Fig. 4 *B*). We conclude that the lipids in the bilayer patch have a similar mobility to those in a much larger SLB.

Correlation between intrinsic curvature and rupture of isolated GUVs

We previously reported that the ability of LUVs to yield fluid planar bilayers is dependent on the average intrinsic curvature, $C_{0,ave}$, and independent of the identity of the component lipids (10). The ''intrinsic curvature'' (C_0) as initially defined by Gruner (28) determines the shape of a completely relaxed, stress-free monolayer. In contrast, the ''spontaneous curvature'' is a different parameter that describes the tendency of a flat bilayer to spontaneously curve to release internal stresses (29). Here, we examined whether the $C_{0,ave}$ plays a role in determining GUV rupture probability. The probability of GUV rupture within 30 min was determined for various combinations of DOPC, DOPE-Me_2, DOPE-Me, and Lyso-PC lipids. Since C_0 values for DOPG and TR-DHPE are not available, we approximated $C_{0,ave}$ by $C'_{0,ave}$ and kept the DOPG and TR-DHPE concentrations constant (Methods). The data indicate that virtually all GUVs with a $C'_{0,ave}$ value of -0.03 to -0.11 nm^{-1} ruptured in 30 min, and those with a $C'_{0,ave}$ value of -0.21 to -0.31 nm^{-1} did not; as the $C'_{0,ave}$ decreased from -0.11 to -0.21 nm^{-1}, the rupture probability progressively decreased (Fig. 5). DOPC/Lyso-PC/DOPG (7:2:1) ($C'_{0,ave} = -0.025$ nm^{-1}) and DOPC/DOPG (9:1) ($C'_{0,ave} = -0.099$ nm^{-1}) GUVs ruptured within 30 min with the same probability of 1.0. However, the probabilities that these GUVs ruptured within 5 min of adsorption were significantly different (0.96 ± 0.05 ($N = 18$) and 0.61 ± 0.09 ($N = 28$), respectively). We conclude that GUV rupture probability depends on $C_{0,ave}$, and that faster rupture occurs at a more positive $C_{0,ave}$.

Since the C_0 of TR-DHPE is expected to be positive due to the large TR dye moiety attached to the lipid headgroup, we considered the possibility that the symmetric rupture events observed with 3 mol % TR-DHPE (Fig. 1 *C*) were a consequence of a larger $C_{0,ave}$, compared with the $C_{0,ave}$ of GUVs with 0.5 mol % TR-DHPE (the $C_{0,ave}$ for DOPC/DOPG (9:1) GUVs with 3 mol % TR-DHPE is expected to be between 0 and -0.1 nm^{-1}) (10). Therefore, we examined the effect of a more positive average intrinsic curvature on the isolated rupture pathway using GUVs that contained Lyso-PC. The formation of planar bilayer patches was observed for DOPC/Lyso-PC/DOPG (8:1:1) and DOPC/Lyso-PC/DOPG (7:2:1) GUVs labeled with 0.5 mol % TR-DHPE ($C'_{0,ave} = -0.062$ and -0.025 nm^{-1},

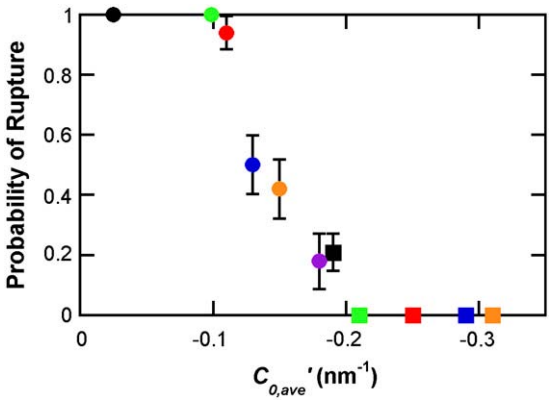

FIGURE 5 Rupture probability dependence on average intrinsic curvature. The probability of GUV rupture was examined 30 min after GUVs with 0.5 mol % TR-DHPE were adsorbed to a glass surface. The $C'_{0,ave}$ values of −0.025 (*black circle*), −0.099 (*green circle*), −0.11 (*red circle*), −0.13 (*blue circle*), −0.15 (*orange circle*), −0.18 (*purple circle*), −0.19 (*black square*), −0.21 (*green square*), −0.25 (*red square*), −0.29 (*blue square*), and −0.31 nm^{-1} (*orange square*) correspond to the following 11 lipid compositions, respectively: DOPC/Lyso-PC/DOPG (7:2:1), DOPC/DOPG (9:1), DOPE-Me$_2$/Lyso-PC/DOPG (7:2:1), DOPE-Me$_2$/Lyso-PC/DOPG (7.5:1.5:1), DOPE-Me$_2$/Lyso-PC/DOPG (8:1:1), DOPE-Me$_2$/DOPC/DOPG (7:2:1), DOPE-Me$_2$/DOPC/DOPG (8:1:1), DOPE-Me$_2$/DOPG (9:1), DOPE-Me/Lyso-PC/DOPG (8:1:1), DOPE-Me/DOPC/DOPG (8:1:1), and DOPE-Me/DOPG (9:1). Scale bars show standard errors. $N = 17$–42.

respectively). All the GUVs examined ($N = 36$ for each lipid composition) ruptured via the asymmetric isolated rupture pathway. These data suggest that it is not the $C_{0,ave}$ alone that leads to the occasional symmetric rupture of GUVs with 3 mol % TR-DHPE.

GUV rupture at higher GUV surface densities

Until now, we have described our observations on the rupture of individual, isolated GUVs on a glass surface. At higher GUV surface densities, it appeared that some GUV rupture events were induced by the contact of GUVs with other lipid structures through at least two mechanisms (Fig. 6). We identified the first mechanism by observing GUVs diffusing near a planar bilayer patch. For isolated DOPC/DOPG (9:1) GUVs, vesicle rupture after adsorption typically occurred on a timescale of minutes. In contrast, GUVs that adsorbed near the edge of an existing planar bilayer patch asymmetrically ruptured in < 1 s after adsorption ($N = 5$). Therefore, rupture occurred significantly faster when GUVs adsorbed near an existing bilayer patch. These data are consistent with a mechanism in which adsorption and deformation proceeded normally but that rupture was induced when the newly arrived GUV interacted with, or near, the edge of an existing bilayer patch (Fig. 6, *A–D*). However, these data do not rule out the possibility that adsorption and deformation could also be influenced by the presence of the existing bilayer patch edge. Vesicles diffusing above a planar bilayer patch but away from the edge of the patch were never observed to rupture.

We identified the second induced rupture mechanism by observing pairs of adsorbed GUVs in which the separation distance was small (approximately less than or equal to a GUV radius). Though the stability of each adsorbed GUV in the pair was consistent with that observed for isolated GUVs (where rupture occurs within minutes after adsorption), rupture of one GUV of the pair often induced the rupture of the second within ~10–20 ms ($N = 10$) (Fig. 6, *E* and *F*). For larger inter-GUV spacings, the ruptures of the GUVs were uncoupled. In these cases, a clear space was observed between the planar bilayer patch formed after one GUV ruptured and the second adsorbed, but unruptured GUV ($N = 17$) (Fig. 6 *G*). These data are consistent with the hypothesis that GUV rupture can be induced by contact with a lipid structure from another GUV undergoing rupture (or, possibly, immediately after rupture) (Fig. 6 *H*). Since the timescale of GUV rupture after adsorption to the glass surface by pathways 3 and 4 was significantly faster ($\leq$ ~1 s) than that by pathway 1 (minutes), the rupture mechanism is likely fundamentally different.

DISCUSSION

The major findings from this study on SLB formation from GUVs are: 1), GUVs rupture by at least four distinct pathways; 2), GUV rupture occurs in ~10–20 ms; 3), GUV rupture begins spontaneously or through contact with external lipid structures, and proceeds by expansion of a single rupture pore; and 4), for the major isolated GUV rupture pathway, the rupture probability is dependent on the $C_{0,ave}$ of the component lipids, and the inner membrane leaflet of the original vesicle becomes exposed to the bulk solution upon conversion into a planar bilayer patch. We now discuss the implication of these results.

Our first major conclusion is that vesicle rupture is initiated by pore formation near the bilayer-glass interface. Isolated GUVs predominantly rupture by growth of a pore that initiates near the edge of the adsorbed bilayer region (asymmetric isolated rupture pathway). One possibility is that rupture pore formation initiates at a region of energetic instability. When a GUV adsorbs to a glass surface, its original spherical structure becomes deformed due to the adhesive forces (30). The most highly curved region in this deformed bilayer structure lies a small distance above the surface near the edge of the adsorbed region. In this highly curved bilayer region, the inner and outer membrane leaflets have significantly higher negative and positive curvatures, respectively, than the near-zero curvatures for both leaflets in a large spherical vesicle. Thus, this highly curved region is energetically unstable (24), and therefore, it is conceivable that isolated vesicle rupture typically begins within or near this region of instability. This energetic instability due to bilayer curvature likely provides a larger

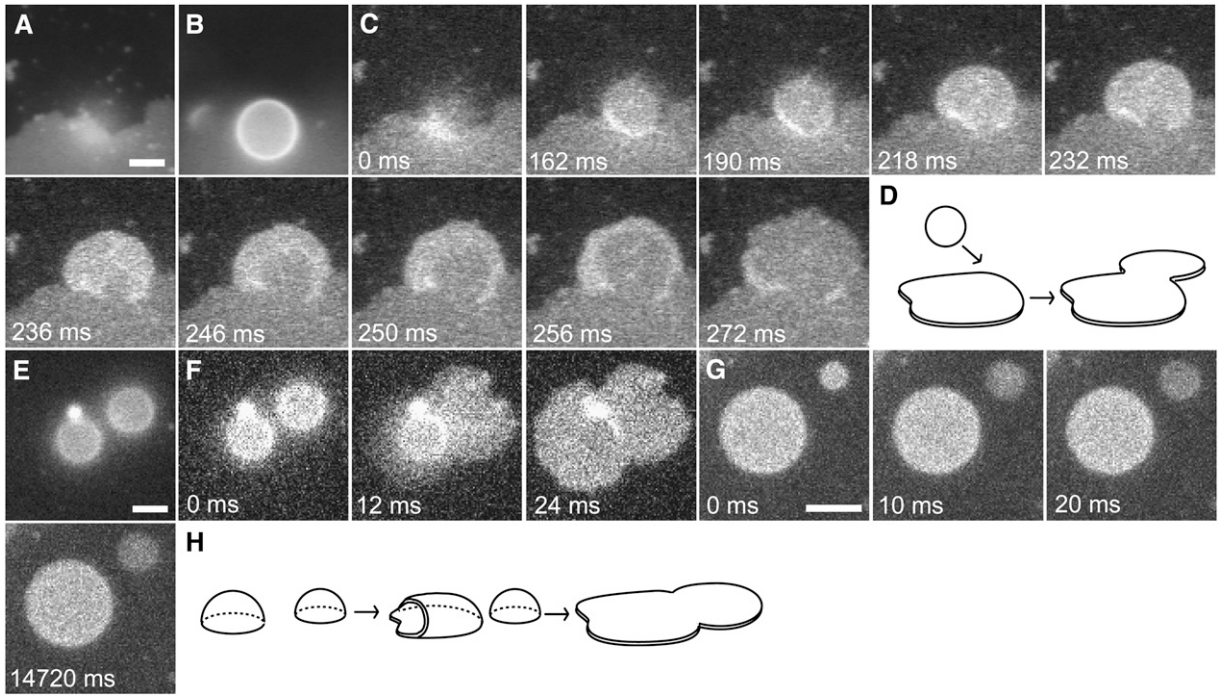

FIGURE 6 Induced GUV rupture. DOPC/DOPG (9:1) GUV rupture was monitored by TR fluorescence (3 mol % TR-DHPE for all images except *E–G*, where the TR-DHPE concentration was 0.5 mol %) under conditions where GUVs could contact other lipid structures. Scale bars, 5 μm. (*A–D*) GUV rupture induced by a planar bilayer edge. Integration times are 64 ms (*A* and *B*) and 2 ms (*C*). (*A*) A planar bilayer patch imaged within the glass-surface focal plane. The large bilayer patch that occupies most of the bottom half of the image probably arose from the fusion of many bilayers from GUVs that ruptured. (*B*) An intact GUV imaged 5 μm above the planar bilayer patch in *A*. (*C*) The GUV from *B* as it diffused down to the glass surface, adsorbed, and ruptured. The pattern of fluorescence intensity changes for the GUV are similar to those shown in Fig. 2 *A*, suggesting a similar rupture process. A movie is available online in Supplementary Material (Fig6C.mov). The focal plane is the glass surface. (*D*) Schematic illustration of the vesicle rupture caused by the interaction between a planar bilayer edge and a GUV. (*E* and *F*) GUV rupture induced by the rupture of a nearby GUV. The focal plane is the glass surface; integration times are 64 ms (*E*) and 12 ms (*F*). (*E*) Two adsorbed GUVs imaged within the glass-surface focal plane. (*F*) Near-simultaneous rupture of the GUVs shown in *E*. Rupture of the GUV on the right (12 ms) was followed almost immediately by rupture of the GUV on the left (24 ms). (*G*) Uncoupled GUV rupture. Rupture of the GUV on the upper right (10 ms) was not followed by rupture of the GUV on the lower left for at least 14.7 s. The focal plane is the glass surface; integration time is 10 ms. (*H*) Schematic illustration of the vesicle rupture caused by the interaction between a GUV and a nearby GUV that spontaneously ruptured, as in *F*.

contribution to rupture probability than membrane tension effects introduced by GUV adsorption to the glass surface or minor differences in internal and external osmotic pressures.

Our second major conclusion is that the $C_{0,\mathrm{ave}}$ exerts a powerful modulating influence on vesicle rupture, and a low $C_{0,\mathrm{ave}}$ can effectively prevent vesicle rupture. We postulate that a low $C_{0,\mathrm{ave}}$ inhibits pore formation. A rupture pore is inherently unstable due to the presence of a bilayer edge. Nonetheless, pores spontaneously open within freely diffusing GUVs (31). We surmise that pores also spontaneously open in adsorbed vesicles. If the spontaneous creation of a sufficiently large pore is accompanied by the adsorption of some additional bilayer area to the surface, a chain reaction could ensue, leading to a larger and larger pore and more and more adsorbed bilayer, since the adsorption free energy could compensate for the increased edge energy. The increased membrane tension and high curvature near the contact line experienced by a strongly adsorbed vesicle would also be relaxed upon vesicle rupture, providing an additional thermodynamic driving force to rupture (14,24). As for freely diffusing GUVs, spontaneous pore openings could be inhibited by negative curvature lipids (31), preventing GUVs with a low $C_{0,\mathrm{ave}}$ from rupturing. Our data support this picture. Further, we hypothesize that spontaneous pore formation occurs most likely at regions of highest instability, consistent with the observation that for most GUVs, rupture appeared to initiate near the edge of the bilayer adsorbed region. Due to the large head group on TR-DHPE, this lipid could quite reasonably partition into the high positive-curvature edge region of a pore structure. However, we did not observe an increased concentration of TR-DHPE at the edges of pores or planar bilayer patches, suggesting that higher partitioning of TR-DHPE into edge regions does not occur. Thus, the cause of the symmetric rupture events observed at 3 mol % TR-DHPE requires further investigation. The observation that GUV rupture probability is inhibited by a lower $C_{0,\mathrm{ave}}$ is consistent with

the hypothesis that there is a higher transition-state barrier to rupture under lower $C_{0,ave}$ conditions. We propose that the primary energetic contribution to this higher transition-state barrier is the large line-tension free energy (G_{line}) of rupture pores in vesicles with low $C_{0,ave}$ (see Supplementary Material).

The data presented here are most consistent with a model of spontaneous isolated GUV rupture in which the vesicle opens somewhat like a flower bud, such that the inner membrane leaflet becomes exposed to the bulk solvent and the outer leaflet becomes adsorbed to the glass surface. Since SLB formation is expected to include induced rupture events (e.g., rupture events catalyzed by the edge of a bilayer patch or by a rupturing vesicle), the origin of the lipids in the two leaflets of the resultant SLB could be largely determined by the induced rupture mechanisms. Due to the technical challenges of determining the origin of lipids with a mixed population of vesicles and observing induced rupture events, which were rare under our dilute conditions, we were unable to determine the orientation of the membrane leaflets for induced rupture events. However, other studies have examined the origin of the two membrane leaflets in planar bilayers. Proteoliposomes from human erythrocyte ghosts formed SLBs on cellulose films such that the outer leaflet was adsorbed to the surface and the inner leaflet was exposed to the bulk solution, consistent with the data presented here (32). In contrast, proteoliposomes containing photosynthetic reaction centers or tissue factor were reported to form SLBs such that the outer vesicle leaflet remained exposed to the bulk solution (3,33). These data suggest the possibility that the vesicle rupture mechanism is dependent on the presence and identity of membrane proteins. Alternatively, considering that the membrane leaflets in induced rupture events could orient opposite to those in spontaneous rupture events, membrane proteins could influence whether the spontaneous- or induced-rupture pathway dominates.

Edges of PC lipid bilayers are unstable since the interaction of the lipids' hydrophobic tails with the aqueous solution is energetically unfavorable and PC is ill-adapted to shield bilayer edges from the aqueous solution (in contrast, positive-curvature lipids can quite efficiently cap bilayer edges, e.g., bicelles (34)). Therefore, the presence of PC bilayer edges are typically minimized through the assembly of extended lamellar sheets or by closed-shell vesicle structures (35). However, the planar bilayer patches observed after single GUV rupture events were present for as long as we examined them (up to $\sim$2 h), indicating that glass-adsorbed bilayer patches are reasonably stable. Calculations support the picture that the adsorption energy is more than sufficient to compensate for the edge energy of large bilayer patches (Fig. S3). The fact remains, however, that the edge exists within the adsorbed structure and the lipids within the bilayer patch are poorly adapted to shield the edge. Under our conditions, the flip-flop of NBD-cap PE in intact vesicles was slow. However, all the NBD-cap PE lipid in a planar bilayer patch was accessible to anti-DNP antibody (see Supplementary Material). We conclude that the two bilayer leaflets must be connected, not by flip-flop, but through diffusion of lipids around the highly curved edge region. Consistent with this notion, it has been argued that lipid flip-flop occurs at membrane defects, often identified as pores (36,37). Though the global planar bilayer patch structure is thermodynamically stable when adsorbed to glass, the edge still is a region of local instability. Thus, the bilayer edge is likely to be highly reactive toward other lipid structures, such as intact vesicles. We conclude that the inherent instability of the bilayer edge is sufficient to induce vesicle rupture, such as those events observed in Fig. 6. However, for the near simultaneous rupture of two adsorbed vesicles (Fig. 6 *F*), it is possible that rupture of the second vesicle is driven by a membrane interaction that does not involve the bilayer edge (e.g., by the forceful collision between two bilayers).

Previous studies have suggested that small vesicles first fuse to form larger vesicles before rupturing (2,6), a picture supported by thermodynamic calculations that indicate that the isolated rupture of small vesicles is energetically unfavorable (Supplementary Material). Namely, it is energetically unfavorable for isolated DOPC or DOPE-Me vesicles of $< \sim 0.3$ μm to rupture and form a planar bilayer patch due to the unfavorable edge energy. However, the fusion of two adsorbed vesicles is energetically favorable (14,30). SLB formation from LUVs follows a dependence on $C_{0,ave}$ (10) similar to what we have observed here for GUV rupture, suggesting that the role of $C_{0,ave}$ is similar for these two processes. Since membrane fusion is enhanced by negative-curvature lipids rather than inhibited by a low $C_{0,ave}$ (38–42), we earlier concluded that the membrane fusion of LUVs was not the SLB formation step dependent on $C_{0,ave}$ (10). If LUVs must first fuse before spontaneous rupture on glass, they effectively become adsorbed GUVs. By using GUVs, then, we have effectively eliminated the possible requirement for vesicle-vesicle fusion when planar bilayer patches are formed from smaller vesicles. Therefore, we postulate that the $C_{0,ave}$ dependence of SLB formation from LUVs stems from the requirement that the LUVs fuse to form adsorbed GUVs, and that rupture of the resultant GUVs is dependent upon formation of a rupture pore, a process that is dependent upon $C_{0,ave}$. Of course, SLB formation requires the rupture of many vesicles to form a continuous bilayer structure. Our experiments indicate that vesicle rupture can be highly cooperative, namely, a GUV can be induced to rupture by a GUV undergoing rupture. It is straightforward to envision, then, that for a surface covered with vesicles, a single vesicle rupture event could initiate a chain reaction of rupture events, leading to rapid SLB formation. When SLBs are formed from LUVs, this chain reaction could involve both LUVs and GUVs (formed by vesicle-vesicle fusion), and could be initiated by spontaneous GUV rupture events.

CONCLUSIONS

This work has identified four distinct pathways by which GUVs can rupture at a glass surface. SLB formation is readily explained by spontaneous initial rupture events, followed by additional rupture events induced by vesicle contact with existing planar bilayer edges. The inhibition of planar bilayer formation by a low $C_{0,ave}$ is attributed to the energetic instability of spontaneous pore formation, which is a prerequisite for spontaneous rupture. We hypothesize that SLB formation from smaller vesicles proceeds in a similar fashion.

SUPPLEMENTARY MATERIAL

An online supplement to this article can be found by visiting BJ online at http://www.biophysj.org.

This work was supported by the Program in Membrane Structure and Function (P.S.C. and S.M.M.), the National Institutes of Health (GM070622 for P.S.C.; GM065534 for S.M.M.), the Welch Foundation (A-1421 for P.S.C.; BE-1541 for S.M.M.), and the Mallinckrodt Foundation (S.M.M.).

REFERENCES

1. Reimhult, E., F. Höök, and B. Kasemo. 2003. Intact vesicle adsorption and supported biomembrane formation from vesicles in solution: influence of surface chemistry, vesicle size, temperature, and osmotic pressure. *Langmuir*. 19:1681–1691.
2. Schönherr, H., J. M. Johnson, P. Lenz, C. W. Frank, and S. G. Boxer. 2004. Vesicle adsorption and lipid bilayer formation on glass studied by atomic force microscopy. *Langmuir*. 20:11600–11606.
3. Salafsky, J., J. T. Groves, and S. G. Boxer. 1996. Architecture and function of membrane proteins in planar supported bilayers: a study with photosynthetic reaction centers. *Biochemistry*. 35:14773–14781.
4. Cremer, P. S., and S. G. Boxer. 1999. Formation and spreading of lipid bilayers on planar glass supports. *J. Phys. Chem. B*. 103:2554–2559.
5. Yang, T., S. Y. Jung, H. Mao, and P. S. Cremer. 2001. Fabrication of phospholipid bilayer-coated microchannels for on-chip immunoassays. *Anal. Chem*. 73:165–169.
6. Johnson, J. M., T. Ha, S. Chu, and S. G. Boxer. 2002. Early steps of supported bilayer formation probed by single vesicle fluorescence assays. *Biophys. J*. 83:3371–3379.
7. Keller, C. A., and B. Kasemo. 1998. Surface specific kinetics of lipid vesicle adsorption measured with a quartz crystal microbalance. *Biophys. J*. 75:1397–1402.
8. Keller, C. A., K. Glasmastar, V. P. Zhdanov, and B. Kasemo. 2000. Formation of supported membranes from vesicles. *Phys. Rev. Lett*. 84:5443–5446.
9. Reimhult, E., F. Höök, and B. Kasemo. 2002. Vesicle adsorption on SiO2 and TiO2: dependence on vesicle size. *J. Chem. Phys*. 117:7401–7404.
10. Hamai, C., T. L. Yang, S. Kataoka, P. S. Cremer, and S. M. Musser. 2006. Effect of average phospholipid curvature on supported bilayer formation on glass by vesicle fusion. *Biophys. J*. 90:1241–1248.
11. Crane, J. M., V. Kiessling, and L. K. Tamm. 2005. Measuring lipid asymmetry in planar supported bilayers by fluorescence interference contrast microscopy. *Langmuir*. 21:1377–1388.
12. Goennenwein, S., M. Tanaka, B. Hu, L. Moroder, and E. Sackmann. 2003. Functional incorporation of integrins into solid supported membranes on ultrathin films of cellulose: impact on adhesion. *Biophys. J*. 85:646–655.
13. Granéli, A., J. Rydström, B. Kasemo, and F. Höök. 2003. Formation of supported lipid bilayer membranes on SiO2 from proteoliposomes containing transmembrane proteins. *Langmuir*. 19:842–850.
14. Lipowsky, R., and U. Seifert. 1991. Adhesion of vesicles and membranes. *Mol. Cryst. Liq. Cryst*. 202:17–25.
15. Hope, M. J., A. L. Bailey, L. D. Mayer, A. S. Janoff, and P. R. Cullis. 1986. Generation of multilamellar and unilamellar phospholipid vesicles. *Chem. Phys. Lipids*. 40:89–107.
16. Hope, M. J., M. B. Bally, G. Webb, and P. R. Cullis. 1985. Production of large unilamellar vesicles by a rapid extrusion procedure. Characterization of size distribution, trapped volume and ability to maintain a membrane potential. *Biochim. Biophys. Acta*. 812:55–65.
17. Kaback, H. R. 1971. Bacterial membranes. *Methods Enzymol*. 22: 99–120.
18. Leighton, F., B. Poole, H. Beaufay, P. Baudhuin, J. W. Coffey, S. Fowler, and C. DeDuve. 1968. The large-scale separation of peroxisomes, mitochondria, and lysosomes from the livers of rats injected with Triton WR-1339. Improved isolation procedures, automated analysis, biochemical and morphological properties of fractions. *J. Cell Biol*. 37:482–513.
19. McKeel, D. W., and L. Jarett. 1970. Preparation and characterization of a plasma membrane fraction from isolated fat cells. *J. Cell Biol*. 44:417–432.
20. Akashi, K., H. Miyata, H. Itoh, and K. Kinosita. 1996. Preparation of giant liposomes in physiological conditions and their characterization under an optical microscope. *Biophys. J*. 71:3242–3250.
21. Fuller, N., and R. P. Rand. 2001. The influence of lysolipids on the spontaneous curvature and bending elasticity of phospholipid membranes. *Biophys. J*. 81:243–254.
22. Keller, S. L., S. M. Bezrukov, S. M. Gruner, M. W. Tate, I. Vodyanoy, and V. A. Parsegian. 1993. Probability of alamethicin conductance states varies with nonlamellar tendency of bilayer phospholipids. *Biophys. J*. 65:23–27.
23. Lewis, J. R., and D. S. Cafiso. 1999. Correlation between the free energy of a channel-forming voltage-gated peptide and the spontaneous curvature of bilayer lipids. *Biochemistry*. 38:5932–5938.
24. Lipowsky, R., M. Brinkmann, R. Dimova, T. Franke, J. Kierfeld, and X. Zhang. 2005. Droplets, bubbles, and vesicles at chemically structured surfaces. *J. Phys. Condens. Matter*. 17:S537–S558.
25. Tocanne, J.-F., L. Dupou-Cézanne, and A. Lopez. 1994. Lateral diffusion of lipids in model and natural membranes. *Prog. Lipid Res*. 33:203–237.
26. Axelrod, D., D. E. Koppel, J. Schlessinger, E. Elson, and W. W. Webb. 1976. Mobility measurement by analysis of fluorescence photobleaching recovery kinetics. *Biophys. J*. 16:1055–1069.
27. Soumpasis, D. M. 1983. Theoretical analysis of fluorescence photobleaching recovery experiments. *Biophys. J*. 41:95–97.
28. Gruner, S. M. 1985. Intrinsic curvature hypothesis for biomembrane lipid composition: a role for non-bilayer lipids. *Proc. Natl. Acad. Sci. USA*. 82:3665–3669.
29. Kozlov, M. M., and D. Andelman. 1996. Theory and phenomenology of mixed amphiphilic aggregates. *Curr. Opin. Coll. Interf. Sci*. 1:362–366.
30. Seifert, U. 1997. Configurations of fluid membranes and vesicles. *Adv. Phys*. 46:13–137.
31. Karatekin, E., O. Sandre, H. Guitouni, N. Borghi, P. H. Puech, and F. Brochard-Wyart. 2003. Cascades of transient pores in giant vesicles: line tension and transport. *Biophys. J*. 84:1734–1749.
32. Tanaka, M., S. Kaufmann, J. Nissen, and M. Hochrein. 2001. Orientation selective immobilization of human erythrocyte membranes on ultrathin cellulose films. *Phys. Chem. Chem. Phys*. 3:4091–4095.
33. Contino, P. B., C. A. Hasselbacher, J. B. A. Ross, and Y. Nemerson. 1994. Use of an oriented transmembrane protein to probe the assembly of a supported phospholipid bilayer. *Biophys. J*. 67:1113–1116.
34. Sanders, C. R., and R. S. Prosser. 1998. Bicelles: a model membrane system for all seasons? *Structure*. 6:1227–1234.

35. Jiang, F. Y., Y. Bouret, and J. T. Kindt. 2004. Molecular dynamics simulations of the lipid bilayer edge. *Biophys. J.* 87:182–192.

36. Raphael, R. M., R. E. Waugh, S. Svetina, and B. Zeks. 2001. Fractional occurrence of defects in membranes and mechanically driven interleaflet phospholipid transport. *Phys. Rev. E.* 64:051913.

37. Wimley, W. C., and T. E. Thompson. 1991. Transbilayer and interbilayer phospholipid exchange in dimyristoylphosphatidylcholine/dimyristoylphosphatidylethanolamine large unilamellar vesicles. *Biochemistry.* 30:1702–1709.

38. Bailey, A. L., and P. R. Cullis. 1997. Liposome fusion. *In* Lipid Polymorphism and Membrane Properties. R. M. Epand, editor. Academic Press, San Diego. 359–373.

39. Chernomordik, L. 1996. Non-bilayer lipids and biological fusion intermediates. *Chem. Phys. Lipids.* 81:203–213.

40. Chernomordik, L. V., S. S. Vogel, A. Sokoloff, H. O. Onaran, E. A. Leikina, and J. Zimmerberg. 1993. Lysolipids reversibly inhibit Ca^{2+} dependent, GTP-dependent and pH-dependent fusion of biological membranes. *FEBS Lett.* 318:71–76.

41. Haque, M. E., and B. R. Lentz. 2004. Roles of curvature and hydrophobic interstice energy in fusion: studies of lipid perturbant effects. *Biochemistry.* 43:3507–3517.

42. Yeagle, P. L. 1997. Membrane fusion intermediates. *In* Lipid Polymorphism and Membrane Properties. R. M. Epand, editor. Academic Press, San Diego. 375–401.